Invited review

Understanding and modeling of gas-condensate flow in porous media

Palash Panja[1,2]*, Raul Velasco[2], Milind Deo[1]

[1]*Department of Chemical Engineering, University of Utah, Salt Lake City, Utah 84112, United States*
[2]*Energy & Geoscience Institute, University of Utah, Salt Lake City, Utah 84108, United States*

Abstract:
Well deliverability impairment due to liquid dropout inside gas-condensate reservoirs below dew-point pressure is a common production problem. The operating conditions and the thermodynamic properties of the condensate govern the production performance of this type of reservoir. Modeling condensate production using analytical, semi-analytical or empirical formula for quick assessment of reservoir performance is a complicated method due to the complex thermodynamic behavior. The objective of this study is to provide a fundamental understanding of the flow and thermodynamics of gas-condensate fluid to develop tools for the production prediction. The prior developments of flow modeling of gas-condensate are briefly reviewed. The multi-phase flow and the depletion stages during production are discussed. Each component of pseudo-pressure calculations to determine the condensate flow rate is explained. Thermodynamic properties and laboratory experiment relevant to the flow of condensate are also explored. Pressure-volume-temperature properties such as two-phase envelope, constant composition expansion and constant volume depletion are demonstrated for three different gas-condensate fluids namely lean, intermediate and rich. This article is also useful for future developments of the production model for a gas-condensate under various operational and completion scenarios such as horizontal wells and hydraulic fractures in tight formations.

1. Introduction

Condensate is a water-white to light straw-colored liquid hydrocarbon which is produced with a large amount of gas. The density of condensate in terms of American Petroleum Institute (API) gravity is usually above 50 degrees and the produced gas-to-liquid ratios in the separator usually range from 10,000 cubic feet to more than 100,000 cubic feet per barrel (Thornton, 1946). The reservoir is often initially filled with gas only. Liquid condensate forms inside the reservoir when the pressure drops below the dew-point pressure and eventually condensate starts flowing with gas (multi-phase) after it exceeds the critical condensate saturation. The magnitude of the pressure decline below the dew-point is one of many factors affecting the amount of condensate drop-out. Therefore, higher condensate drop-out is usually observed near the wellbore or hydraulic fractures in tight formations due to a sharp decline in pressure. This impairs the liquid production due to its low mobility compared to gas. The extent of blockage depends on various factors such as Pressure-volume-temperature (PVT) properties, absolute permeability of the rock, relative permeability and, well operational conditions. Understanding and modeling of the two-phase flow of gas and condensate in porous media are challenging tasks due to the complex interactions among the influencing factors. Numerous production analysis techniques and models have been developed since the early studies on oil flow in conventional reservoirs (Millikan, 1926; Coleman et al., 1930). These studies can be broadly categorized such as empirical formulation like decline curve and type curve analysis, surrogate models, material balance methods, numerical simulation, pore network model (PNM), and semi-analytical methods.

On the other hand, the decline curve analysis (DCA) method has been used for a long time for its rapid predictive capability. Arps (1945) developed the first mathematical model including exponential decline, hyperbolic decline, and harmonic decline by fitting them with available production data.

Ausasia Science and Technology Press

$$\text{Exponential: } q = q_i e^{-D_i t} \qquad (1)$$

$$\text{Hyperbolic: } q = q_i (1 + b D_i t)^{-\frac{1}{b}}, \; 0 < b < 1 \qquad (2)$$

$$\text{Harmonic: } q = q_i (1 + D_i t)^{-1} \qquad (3)$$

where D_i is defined as the initial flow rate changed in unit time:

$$D_i = -\left(\frac{1}{q} \frac{\partial q}{\partial t} \right)_{t \to 0} \qquad (4)$$

After finding the fitted parameters (b and D_i) using regression with production history, it is used to predict the flow rate. It is also used to calculate the estimated ultimate recovery (EUR) using the cumulative production curve by extending it until the time where the flow rate reaches the uneconomic limit of production. Consequently, other new and modified versions of Arp's method (Mead, 1956; Mannon, 1965; Fetkovich, 1980) were developed. Most decline curves are constructed based on the single-phase boundary dominated flow in a conventional reservoir with high permeability (milli Darcy range). Therefore, they are not applicable to transient flow with moving boundaries such as the case of unconventional reservoirs with ultra-low matrix permeability (micro to nano Darcy range). A few new techniques have been emerged to fit the production data from tight formations such as the Power Law Exponential (PLE) (Ilk et al., 2008), Stretched-Exponential model (SE) (Valko, 2009), Logistic Growth Analysis (LGA) (Clark et al., 2011) and Duong Method (Duong, 2010). No reservoir parameters are included in all these DCA models, therefore, they can not be used for reservoir characterization such as permeability estimation or fracture length determination in tight formation. Alternatively, type curves are developed (Fetkovich, 1980; Palacio and Blasingame, 1994; Agarwal et al., 1999; Pratikno et al., 2003) for the estimation of permeability, skin, drainage radius, and fracture half-length. However, type curves are also based on the single-phase Darcy flow with pressure independent permeability. The effects of stress/pressure on permeability, porosity, and relative permeability were demonstrated experimentally (Fatt and Davis, 1952; Fatt, 1953; Vairogs et al., 1971; Thomas and Ward, 1972; McKee et al., 1988; Kikani and Pedrosa, 1991; Rushing et al., 2007; Dong et al., 2010). Therefore, these parameters consequently affect the production of hydrocarbon (Thompson et al., 2010; Okouma Mangha et al., 2011; Clarkson et al., 2013). Researchers (Johnson and Jamiolahmady, 2018) modified type curves incorporating the effects of pressure on permeability (Raghavan et al., 1972; Ostensen, 1986; Thompson et al., 2010; Clarkson et al., 2013) and porosity. Despite all recent development of DCA and type curves to forecast oil and gas flow rates in tight/shale reservoirs, they are empirically developed and sometimes predict unrealistic or infinite EUR.

Surrogate models (Amorim and Schiozer, 2012; Dahaghi et al., 2012) such as polynomial functions (Parikh, 2003; Li and Friedmann, 2005; Carreras et al., 2006; Panja and Deo,

2016) and machine learning algorithms (El-Sebakhy, 2007; Anifowose et al., 2011; Panja et al., 2016) are useful in determining the production performance for a set of geologic, completion, and operational parameters (Panja et al., 2016). The main drawback of surrogate models is the requirements of various model parameters along with the availability of high-performance computers.

The general material balance equations in the oil and gas industry based on hydrocarbon volume balance are initially presented by Schilthuis (1936). The general material balance method has three main unknown namely average reservoir pressure, recovery factor, and cumulative gas oil ratio (GOR). Other parameters can be expressed as the functions of pressure. Many integrated approaches (Tarner, 1944; Muskat, 1945; Tracy, 1955) were developed for the prediction of production performance using the material balance equation in the solution-gas-drive reservoir. Havlena and Odeh (1963) first re-arranged the material balance equation as a straight line and fitted it with the field production data. The linear form is useful for calculations of initial oil in place, gas cap size, water influx, and drive mechanisms. The general material balance method works well on the assumption that the reservoir is under uniform average pressure. This is the case for conventional reservoir with boundary dominated flow. However, the unconventional reservoirs such as shales or tight formations have shown different flow behaviors (Orangi et al., 2011; Panja et al., 2016; Panja and Deo, 2016). A semi-analytical method coupled with material balance was developed to predict the production performance in tight formations (Velasco et al., 2016) which is discussed later.

PNM has recently gained interest in studying the effects of nano-pores on PVT properties and multi-transports phenomena like adsorption of gas in organic matter in tight formations. Various pore-network models for two-phase flow of gas-condensate were developed including compositional simulation (Santos and Carvalho, 2020). The effects of condensate saturation on Knudsen flow in kerogen (Labed et al., 2018), flow rate, and interfacial tension on relative permeabilities (Momeni et al., 2017), confinement on phase properties and multi-transports such as free gas transport, gas adsorption, and surface diffusion (Liu et al., 2019; Pan et al., 2019) were also investigated using PNM. Different aspects of PNM can be found in a review article (Xiong et al., 2016). Although the PNM is elegant to capture the multi-physics transports in nano-pores, complex pore networks of real porous media such as microscopic features cannot be represented. The entire workflow of model development and running simulations is complex and time-consuming.

The numerical methods as the alternative to the analytical solution are popular in the oil and gas industry. Fundamental flow equations (partial differential equations) are numerically solved after discretizing using various techniques such as finite difference, finite elements, etc. The control volume finite element (CVFE) method on unstructured grids was developed to simulate gas cycling in a rich retrograde condensate reservoir (Chen et al., 2006). Among the few early studies, numerical simulations were conducted for radial gas condensate well by Eilerts et al. (1965) and Kniazeff and Navilee (1965).

Table 1. Compositions and critical properties of three different condensates, lean, intermediate and rich.

Components	Composition (mole %)		
	Lean	Intermediate	Rich
C1	72.49	67.57	64.52
C2	7.16	7.01	6.91
C3	6.01	5.89	5.81
iC4	1.20	1.07	0.98
nC4	1.99	1.9	1.84
iC5	0.93	0.84	0.78
nC5	0.99	0.89	0.82
FC6	1.39	1.33	1.29
C7+	5.56	11.23	14.78
CO_2	2.14	2.14	2.14
N_2	0.13	0.13	0.13
C7+ Mol. Wt.	129	140	148
C7+ Sp. Gr.	0.775	0.778	0.780

Gondouin et al. (1967) modified the numerical program developed by Kniazeff and Naville (1965) and compared results with field measurements. Fussel (1973) developed a compositional simulator for 1-D radial flow in gas condensate reservoirs and proved that the steady-state predictions were incorrect especially when the reservoir average pressure is below saturation pressure. The equation of state model for gas-condensate fluid was modified in a numerical simulator to accommodate multilayer adsorption in nano-scale pores in an unconventional reservoir (Dong et al., 2016). Isotherm of capillary condensation is computed considering this effect of adsorption (wetting) film. The effect of geomechanics on the production of condensate can not be ignored. In another numerical model, the effect of adsorption on primary recovery and CO_2 enhanced recovery was investigated using an extended Langmuir model and geomechanics (Yang et al., 2019). However, fine grid, multiphase and compositional simulations require longer run time and high computing power.

Developing an analytical model requires an understanding of the flow mechanism inside porous media. The main focus of this mini-review study is to discuss analytical approaches to model gas and condensate flow rates. First, we have discussed the thermodynamical of gas-condensate, i.e., PVT properties. Then, we have described different depletion stages and multiphase flow that are essential in developing a quick prediction tool for production performance. Finally, different models, their drawbacks, and assumptions are discussed.

2. Pressure-volume-temperature

Low gravity liquids like volatile oils and gas condensates can exist in the gas phase in vaporized form. They often show similar thermodynamics properties despite the different initial conditions and flow performance in the reservoir (Panja et al., 2019). The vaporized liquid in the gas phase is first conceptualized by Cook et al. (1974) for gas injection system

and the term volatilized oil (or condensate) to gas ratio (R_v) was applied to conventional material balance equation by Fetkovich et al. (1986). Therefore, modified black oil (MBO) PVT includes the volatilized condensate to gas ratio (R_v) which is used in all the calculations of flow models.

To demonstrate PVT properties, three different gas-condensate fluids with the varying richness of liquid content in the gas are considered. The hydrocarbon compositions are partly taken from Whitson and Sunjerga (2012) as given in Table 1 which represents the plausible compositions of condensate window in Eagle Ford formation, Texas, USA. The components up to carbon number 6, i.e., methane (C1), ethane (C2), propane (C3), iso & normal butane (iC4 and nC4), iso & normal pentane (iC5 and nC5) and, the total fraction of hexane (FC6) are listed in Table 1. All the hydrocarbons heavier than carbon number 6 are lumped together to create a pseudo component C7+ which is characterized by its mole fraction, molecular weight and specific gravity.

For rich gas-condensate fluid, the amount of lighter hydrocarbons is less and the amount of heavier hydrocarbons is high. Thus, mole fraction, the molecular weight and specific gravity of C7+ increase with the richness of the gas-condensate fluids. The two-phase diagram or pressure-temperature (PT) diagram is useful to determine the condensate window for the fluid. The reservoir is ideally considered as an isothermal system of porous media assuming no heat flow using steam or other means. In the PT diagram, when the reservoir temperature is higher than the critical temperature and lower than the cricondentherm (the maximum temperature in the diagram), fluid is characterized as gas condensate. The fluid remains in the gaseous phase when the reservoir pressure is above the dew-point pressure (at reservoir temperature). Liquid condensate forms and drops out from the gaseous phase during production when the reservoir pressure drops below dew-point pressure. This phenomenon is counter-intuitive. Usually, liquid forms
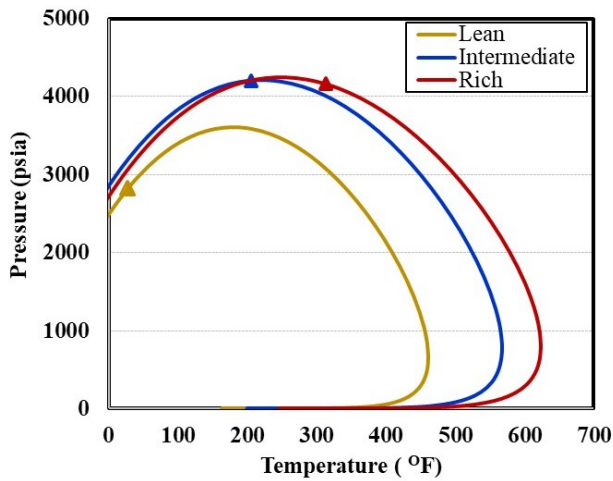
Fig. 1. Two-phase PT diagram for lean, intermediate and rich gas condensates. The critical points are shown using triangular markers.

from the gaseous phase when the system is pressurized at certain temperature conditions. However, in the gas-condensate system, lowering the pressure causes the formation of liquid condensate. For this reason, this fluid is often known as retrograde gas-condensate.

The shape of the PT diagram is dependent on the initial compositions of the reservoir fluid. Two-phase PT boundaries (PT diagram) for lean, intermediate and rich condensate are prepared using Peng-Robinson (1978) equation of state in commercial software Winprop from Computer Modeling Group (CMG), Calgary, Canada as shown in Fig. 1.

Rich condensate has a wider PT diagram with the highest cricondentherm. On the other hand, the lean condensate has a narrower PT diagram with the lowest cricondentherm. Therefore, the rich condensate fluid has a higher dew-point temperature for the same pressure. The amounts of liquid dropout below the dew-point pressure at constant temperature

are important to characterize the flow of liquid condensate. This occurs inside the reservoir during various depletion stage. Two laboratory tests among many namely, constant composition expansion (CCE) and constant volume depletion (CVD) are important to measure the amount of liquid dropout in a gas-condensate fluid. The detailed descriptions of these tests can be found in the literature (Ahmed, 2010; McCain, 2017). The schematics of the CVD experiment are shown in Fig. 2.

A certain amount of representative sample of original reservoir fluid is charged in a visual PVT cell. The temperature of the cell is maintained at reservoir temperature throughout the experiment. At the starting of the experiment, the pressure in the cell is set at dew-point pressure (P_{dew}) and the initial volume of this saturated fluid is considered a reference volume. The pressure inside the cell is reduced below dew-point pressure by removing mercury from the cell as shown in the second schematic in Fig. 2. Therefore, liquid condensate drops out from the gas phase due to the pressure reduction below dew-point pressure. The gas volume (V_g) and the volume of the retrograde liquid (V_L) are visually measured. The cell is brought to the initial total volume by re-injecting mercury and releasing some gas simultaneously to keep the pressure the same. The steps are repeated with reduced pressures. This process is similar to gas production with immobile liquid (due to liquid saturation below the critical liquid saturation) staying in the reservoir below dew-point pressure.

If V_{roCVD} data are not available from experiments but the black-oil PVT properties are available, the following method is followed (Fevang and Whitson, 1996) to calculate the CVD data:

$$(V_{roCVD})_k = \frac{N_{k-1} - G_{k-1}(R_v)_k}{1 - (R_s R_v)_k}(B_o)_k \qquad (5)$$

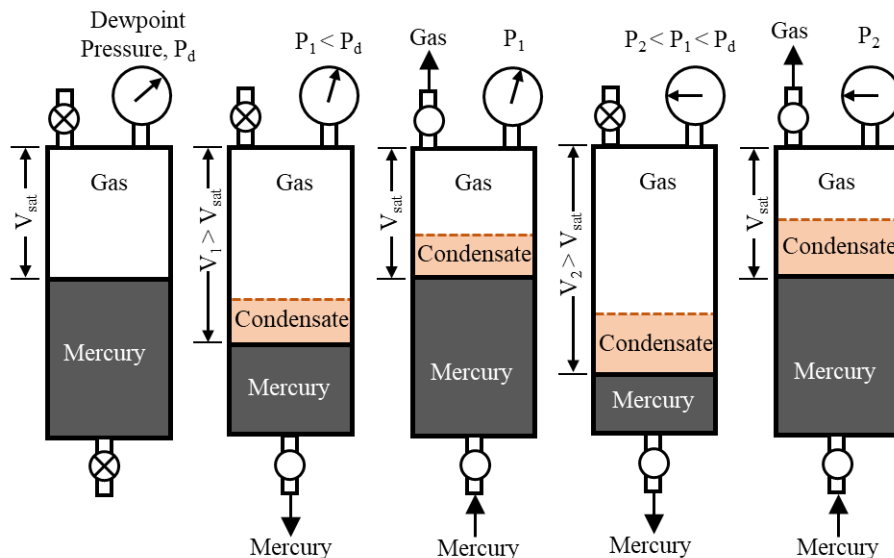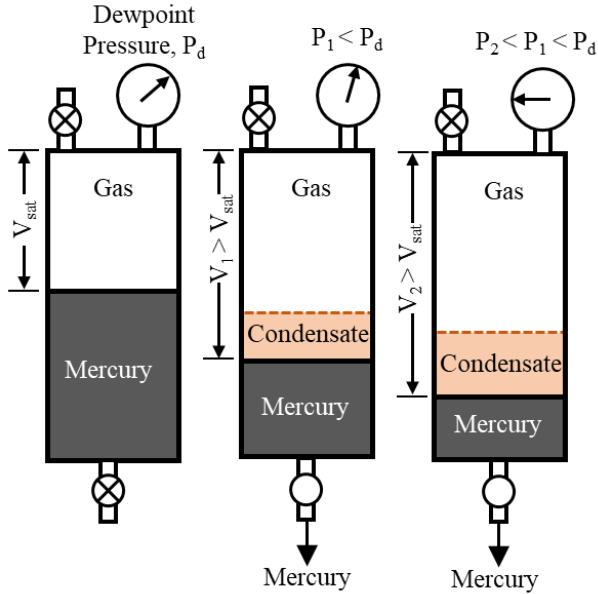$$N_{k-1} = \left(\frac{V_{roCVD}}{B_o} + \frac{1 - V_{roCVD}}{B_{gd}}R_v\right)_{k-1} \qquad (6)$$

Fig. 2. Different steps of CVD test in a laboratory.

Table 2. Theoretical response values for the various algorithms.

Parameters	Lean	Intermediate	Rich
Critical temperature, T_c (°F)	28	205	314
Critical pressure, P_c (psi)	2826	4203	4161
Reservoir temperature (°F)	290	360	396
Dew-point pressure, p_{dew} (psia)	3246	3755	3812
Initial solution CGR (STB/MMSCF)	63	164	244
Maximum CVD liquid dropout (%)	4.4	12.8	20.7

Fig. 3. Different steps of CCE test in a laboratory.

$$G_{k-1} = \left(\frac{V_{roCVD}}{B_o} R_s + \frac{1 - V_{roCVD}}{B_{gd}} \right)_{k-1} \quad (7)$$

The calculation starts from $(V_{roCVD})_0 = 0$ at $P = P_d$. Where k represents the current calculation stage and $k-1$ represents the previous stage. The CCE test procedure is shown in Fig. 3.

The experimental procedure for constant composition expansion is similar to CVD except no hydrocarbon is removed from the PVT cell, thus the overall compositions (combining gas and liquid) are constant during the test. The pressure in the cell is reduced below dew-point pressure by removing mercury from the bottom at the isothermal condition. The total volume of the hydrocarbon is recorded. The ratio of total volume and reference volume, i.e., volume at dew-point pressure is measured as a function of pressure.

Without any experimental data, a fractional amount of condensate (V_{roCCE}) of CCE can be calculated from black oil PVT properties as follows (Fevang and Whitson, 1996):

$$V_{roCCE}(P) = \left[1 + \left(\frac{R_p - R_s}{1 - R_v R_p} \right) \frac{B_{gd}}{B_o} \right]^{-1} \quad (8)$$

where, $V_{roCCE} = V_o / (V_g + V_o)$.

Liquid dropouts during CVD and CCE for three different gas-condensate fluids are prepared using Winprop from CMG, Calgary, Canada as shown in Fig. 4.

The amounts of liquid dropout in CVD and CCE increase with decreasing pressure. However, the liquid dropout reaches a maximum value at a certain pressure and then declines. Liquid volume fractions near dew-point pressure are the same for CVD and CCE experiments. The dew-point pressure can be altered by changing the temperature of experiments. The liquid fractions decrease in CCE experiments with the lower dew-point pressures. The phase behaviors of lean, intermediate and rich condensate are summarized in Table 2.

3. Depletion mechanism

The reservoir may have one or more co-existing regions of single phase or multi-phase depending on the depletion stage. The characteristics of each region and method to calculate pseudo pressure are discussed here.

3.1 Region 1

This is a multi-phase flow region where both gas and liquid condensate are mobile. This saturated region usually appears near the wellbore with pressure below dew-point and the condensate saturation exceeding the critical saturation (i.e., minimum saturation when condensate starts flowing). The maximum pressure where the condensate saturation exceeds its critical saturation is designated as P_1. Therefore, the region is extended from the inner boundary of the wellbore with flowing bottom hole pressure, P_{wf} to the outer boundary with pressure P_1.

In the pseudo pressure calculation in region 1, another main concern is to calculate the relative permeability of gas (k_{rg}) and condensate (k_{ro}) separately as a function of pressure. Because the relative permeabilities are not directly functions of pressure, they can be expressed in terms of PVT properties which are dependent on pressure. It can easily be shown that for two-phase flow, the ratio of relative permeability can be expressed as (Fetkovich et al., 1986):

$$\frac{k_{rg}}{k_{ro}}(P) = \left(\frac{R_p - R_s}{1 - R_v R_p} \right) \frac{\mu_g B_{gd}}{\mu_o B_o} \quad (9)$$

If produced gas condensate ratio (R_p) is known, the right-hand side of Eq. (9) can be calculated using PVT data. The
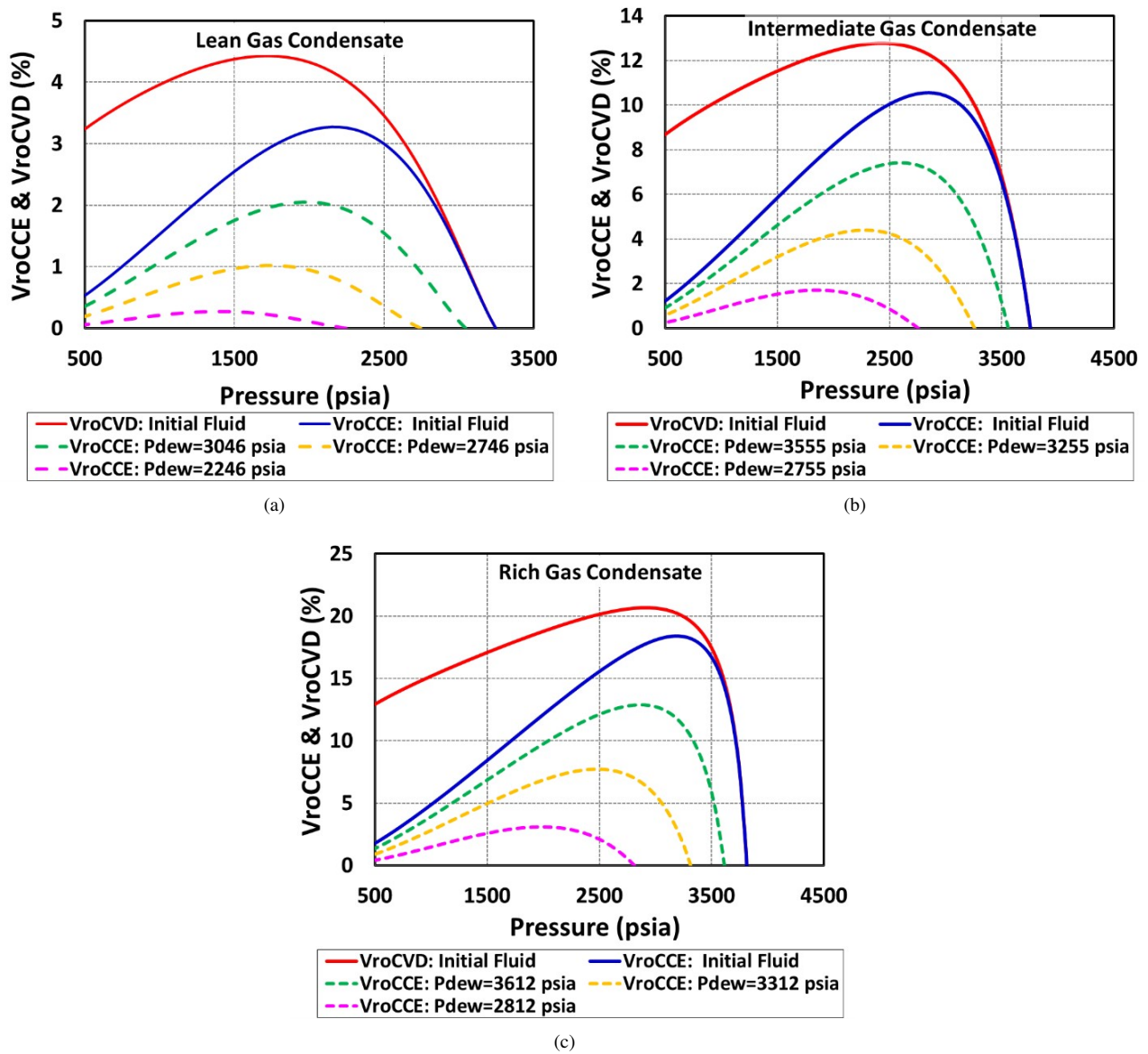
Fig. 4. CVD and CCE for (a) lean; (b) intermediate; (c) rich gas condensate fluids.
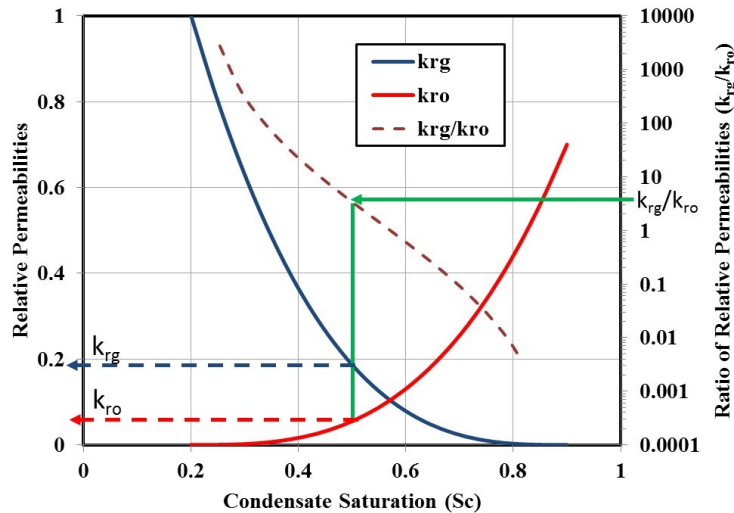

Fig. 5. Relative permeabilities of gas and condensate and the ratio of relative permeabilities.

flow behavior in region 1 is similar to a CCE system. Therefore, the ratio of relative permeability can alternatively be calculated from the fractional amount of condensate (V_{roCCE}) as follows (Fevang and Whitson, 1996):

$$\frac{K_{rg}}{K_{ro}}(P) = \left(\frac{1}{V_{roCCE}} - 1\right)\frac{\mu_g}{\mu_o} \qquad (10)$$

Once the ratio is known, the individual values of relative permeability are obtained from mapping the value in relative permeability curves as shown in Fig. 5.

The procedure is shown through the green solid line. The procedure is also used to calculate the condensate saturation in region 1 for a given pressure.

3.2 Region 2

Like region 1, this is also a two-phase region but only gas flows and the liquid remains immobile due to the low condensate saturation below the critical saturation. The pressure in this region varies from P_1 to the dew-point pressure (P_{dew}). In the regions 1 and 2, the gas contains less volatilized condensate as some of the condensates drop out as liquid phase. To calculate the gas relative permeability K_{rg}, condensate saturation (S_c) must be known as a function of pressure. Because region 2 behaves like a CVD system, condensate saturation as a function of pressure can be obtained from CVD data (Fevang and Whitson, 1996):

$$S_c(p) = V_{roCVD}(1 - S_w) \qquad (11)$$

where, $V_{roCVD} = V_o(p)/V_d$.

Once condensate saturation is known at a particular pressure, gas relative permeability (K_{rg}) is determined from Fig. 5.

3.3 Region 3

Single-phase gas exists and flows in this region because the pressure is higher than the dew-point pressure. This is an undersaturated region thus no liquid condensates are generated. The pressure ranges from dew-point pressure (P_{dew}) to the outer boundary pressure of the reservoir i.e., the initial reservoir pressure ($P_{initial}$) for transient state flow. Because the gas saturation is constant in this region and gas relative permeability is also constant and is calculated from gas-water relative permeability curves at the connate water saturation.

3.4 Region 4

In the case of a tight formation, the outer portion of the reservoir commonly exists in transient state conditions when all parts of the reservoir are not exploited. The boundary of this zone starts when the initial reservoir pressure is first detected to the external boundary of the reservoir. The entire region holds the initial reservoir conditions and is unproductive. Region 4 usually doesn't exist in a conventional reservoir.
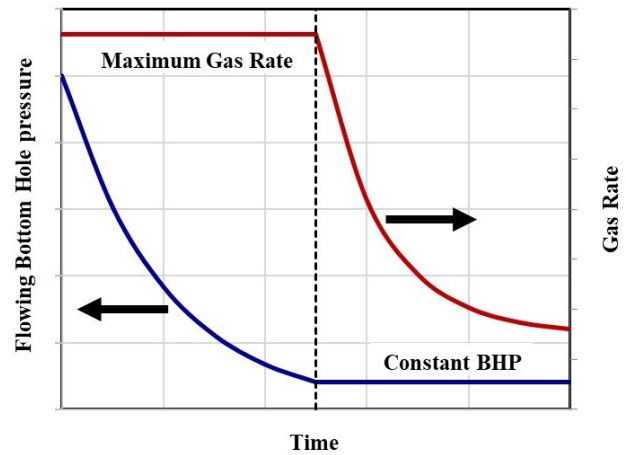

Fig. 6. A typical operating condition of a gas-condensate well with a constant plateau of the gas rate at the starting and the constant minimum flowing bottom hole pressure at the end.

Operating a well in a gas-condensate reservoir is a challenge to engineers. Production optimization is a difficult task due to complicated phase and flow behaviors. Operating well at higher pressure above dew-point pressure seems advantageous because of the single-phase flow of gas without losing any liquid inside the reservoir. However, higher bottom hole pressure means lower drawdown and thus the gas flow rate is low. On the contrary, to increase flow rate drawdown is increased by decreasing bottom hole pressure often below dew-point pressure which leads to liquid dropout. As a result, the remaining gaseous phase holds a lesser amount of volatilized liquid. Due to higher mobility, gas dominates the two-phase flow suppressing the production of liquid condensate. Therefore, the productivity of liquid condensate is reduced in either way. This reduction is dependent on the compositions of the gas-condensate fluid, relative permeabilities, and operating conditions.

Ideally, well can be operated as constant flowing bottom hole pressure (P_{wf}) or constant flow rate. However, a typical operating condition in the real field is shown in Fig. 6.

In the case of constant flow rate operation, the flowing bottom hole pressure (P_{wf}) changes with time. Due to the production of fluids, reservoir pressure drops, therefore, the flowing bottom hole pressure (P_{wf}) is reduced slowly to keep a constant flow rate maintaining constant drawdown. When the flowing bottom hole pressure reaches minimum allowable flowing bottom hole pressure as shown in Fig. 6, production starts decreasing.

The coexistence of various regions is determined by the relative locations of dew-point pressure (P_{dew}), outer boundary pressure of region 1 (P_1) and the flowing bottom hole pressure (P_{wf}). The depletion conditions can be broadly identified into three stages. The co-existence of different regions in each stage is illustrated in Fig. 7.

The flowing bottom hole pressure starts generally above the dew-point pressure ($P_{wf} > P_{dew}$) and it eventually drops below the dew-point pressure ($P_{wf} < P_{dew}$). If the initial flowing bottom hole pressure is above the dew-point pressure, the
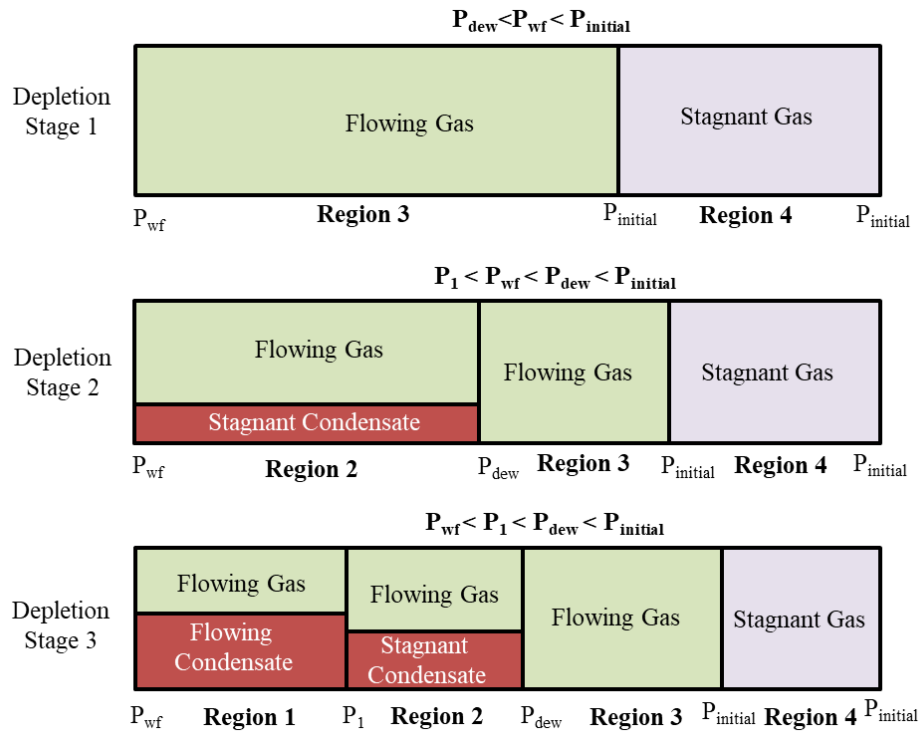
Fig. 7. Appearance of flow regions 1, 2 and 3 in various depletion stages during production.
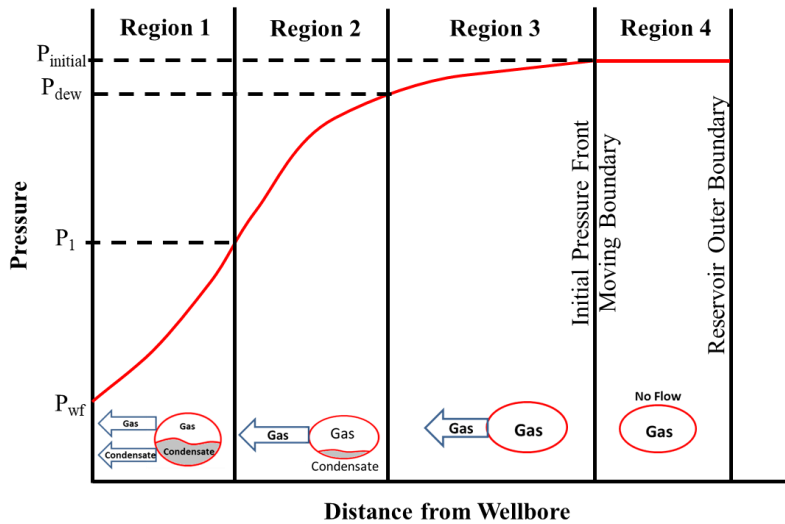

Fig. 8. Pressure profile, physical conditions, and flowability gas and condensate present in region 1, region 2, region 3 and region 4 during bottom hole pressure below dew-point pressure.

reservoir only contains gas (regions 3 and 4), this depletion state is designated as stage 1. In the 2nd depletion stage, flowing bottom hole pressure (P_{wf}) drops below dew-point pressure (P_{dew}) but stays above P_1. Region 2 appears along with region 3 in the outer portion of the reservoir. Since the P_{wf} is higher than P_1, condensate is immobile, and region 1 doesn't exist. In depletion stages 3, the P_{wf} is less than P_1 and the pressure is enough low to generate sufficient liquid condensate to flow, therefore all four flow regions (1, 2, 3 and 4) appear as illustrated in Fig. 8.

It is a primary concern to determine the depletion stage at any time step to calculate the pseudo pressure in Eq. (13) in the next section. This depletion mechanism is simplified considering the idealistic situation. One stage may exist for the entire life of production.

4. Flow Modeling

Several studies have been conducted in the modeling of saturated conventional reservoirs in primary production. The

Table 3. Limits of integration for pseudo pressure calculations for different stages.

Stage	Region 1		Region 2		Region 3	
	Lower	Upper	Lower	Upper	Lower	Upper
1	Doesn't exist	Doesn't exist	Doesn't exist	Doesn't exist	P_{wf}	P_e
2	Doesn't exist	Doesn't exist	P_{wf}	P_{dew}	P_{dew}	P_e
3	P_{wf}	P_1	P_1	P_{dew}	P_{dew}	P_e

gas flow rate (q_g) is calculated from the productivity index (γ_g) and pseudo pressure $(\Delta m(P))$ as:

$$q_g = \gamma_g \Delta m(P) \tag{12}$$

The concept of pseudo pressure is not new; it is generally used for gas flow performance where actual pressure is replaced by pseudo pressure. Mathematically pseudo pressure is expressed as:

$$m(P) = 2 \int_{P_{ref}}^{P} \frac{P dP}{\mu Z} \tag{13}$$

It can easily be realized during solving flow equations that it is advantageous to express all flow equations in terms of these pseudo pressures. Evinger and Muskat (1942) introduced the concept of theoretical productivity factor using pseudo-pressure for solution gas drive reservoirs in steady-state conditions. They proposed an equation for steady-state liquid flow rate from a vertical well with the radial flow using pseudo-pressure as following:

$$q_l = \frac{2\pi h k_o}{\log\left(\frac{r_e}{r}\right)} \int_{P}^{P_{eff}} \frac{k_{rl}}{\mu B} dP \tag{14}$$

This is the constant volume depletion material balance method (CVDMB) (Evinger and Muskat, 1942) where the entire reservoir is considered as homogeneous at any time and the reservoir is characterized by its average pressure. O'Dell (1967) first introduced a pseudo-pressure function to calculate the gas rate in gas-condensate reservoirs in undersaturated conditions. Jones and Raghavan (1988) also presented the concept of the pseudo pressure integral to capture the effect of multiphase flow by modifying the gas pseudo pressure. The gas flow rate in the multiphase flow system of gas-condensate is presented in Eq. (15).

$$q_g = \gamma_g \int_{P_{wf}}^{P_e} \left(\frac{K_{ro}}{B_o \mu_o} R_s + \frac{K_{rg}}{B_{gd} \mu_g} \right) dP \tag{15}$$

The productivity index (γ_g) for pseudo-steady state flow is dependent on the choice of the upper limit of integration. Reservoir average pressure (P_R) and external boundary pressure (P_e) are the two most commonly used pressure. For pseudo-steady state flow in a radial reservoir, if average pressure (P_R) is used as the upper limit of integration, $\gamma_g = 2\pi a_1 h k / [\log(r_e/r_w) - 0.75 + s]$; if external boundary pressure (P_e) is used as the upper limit of integration, $\gamma_g = 2\pi a_1 h k / [\log(r_e/r_w) - 0.5 + s]$. Where, a_1 is unit correction factor, for filed unit, $a_1 = 1/(2\pi 141.2)$, for SI unit, $a_1 = 1$.

Fevang and Whitson (1996) modified CVDMB and divided the reservoir into three regions and accordingly, they split the pseudo pressure Eq. (15) into three parts as shown in Eq. (16).

$$\Delta m(P) = \int_{P_{wf}}^{P_e} \left(\frac{K_{ro}}{B_o \mu_o} R_s + \frac{K_{rg}}{B_{gd} \mu_g} \right) dP$$
$$= \int_{P_{wf}}^{P_1} \left(\frac{K_{ro}}{B_o \mu_o} R_s + \frac{K_{rg}}{B_{gd} \mu_g} \right) dP + \int_{P_1}^{P_{dew}} \frac{K_{ro}}{B_{gd} \mu_g} dP$$
$$+ K_{rg} S_{wc} \int_{P_1}^{P_{dew}} \frac{1}{B_{gd} \mu_g} dP \tag{16}$$

As described earlier that gas and condensate both flow in the first region near the wellbore. Gas and condensate both exist in the second zone but only gas flows. In the third zone, only gas exists and flows. This method is applicable in pseudo-steady state conditions for both vertical well and horizontal well with the vertical fracture. The limits of the integration change with the depletion stage. Limits are summarized in Table 3.

The reservoir boundary pressure (P_e) declines with time as reservoir fluid is extracted for a depleted reservoir. Otherwise, the boundary of initial pressure (P_i) moves outward away from the wellbore in the case of an infinite reservoir. Dew-point pressure (P_{dew}) of the reservoir is considered constant to its initial dew-point pressure. Reservoir pressure at any point at any time is bounded by the flowing bottom hole pressure $(P_{wf}$ which is minimum pressure) and the reservoir boundary pressure (P_e).

The upper limit of the integration in region 1 (or lower limit in region 2), i.e., P_1 is not known in the pseudo pressure calculation. P_1 can be evaluated through the estimation of flowing condensate to gas ration (CGR) at the wellbore and in region 1. Fevang and Whitson (1996) considered constant flowing CGR (R_{vf}) in region 1 which is equal to the condensate to gas ratio (R_v) in the deep reservoir at the pressure P_1. Therefore, the produced CGR (the inverse of produced GOR, $1/R_p$) in the well stream is equal to the flowing gas condensate ratio (R_v) at pressure P_1 which is determined from PVT table as:

$$R_v(P_1) = \frac{1}{R_p} \tag{17}$$

Different methods were developed to calculate producing GOR. Fevang and Whitson (1996) obtained the producing GOR (R_p) using a commercial simulator. Guehria (2000) followed the same method except that producing GOR (R_p) is calculated from Muskat (1945) material balance method modified for gas condensate system as shown in Eq. (18).

$$R_p = \frac{\left(-\frac{1}{B_g} + \frac{R_s}{B_o}\right)\frac{dS_o}{dp} - S_o\left[\frac{d}{dp}\left(\frac{1}{B_g}\right) - R_s\frac{d}{dp}\left(\frac{1}{B_o}\right) - \frac{1}{B_o}\frac{dR_s}{dp}\right]}{\left(-\frac{R_v}{B_g} + \frac{1}{B_o}\right)\frac{dS_o}{dp} + S_o\left[\frac{d}{dp}\left(\frac{1}{B_o}\right) - R_v\frac{d}{dp}\left(\frac{1}{B_g}\right) - \frac{1}{B_g}\frac{dR_v}{dp}\right]}$$
(18)

The Eqs. (9) and (18) can be solved simultaneously for two unknowns (R_p and condensate saturation, S_o). The derivative term of PVT properties is determined from the slope. The saturation derivative is discretized for two pressure steps. The condensate saturation starts with zero value at dew-point pressure. Subsequently, the GOR and condensate saturation are calculated for a given pressure.

Mott (2003) showed that the above method overestimated the flowing CGR. A new method was developed to estimate flowing GOR based on the growth of the region 1 using a material balance as shown in Eq. (19).

$$\Delta PV (S_{o,1} - S_{o,2})\left[\frac{1}{B_o(P_1)} - \frac{R_v(P_1)}{B_g(P_1)}\right]$$
$$= \left\{q_{o,\max} - q_{qw}R_v(P_1)\left[1 - \frac{PV(P_1)}{PV_{tot}}\right]\right\}\Delta t$$
(19)

The condensate saturation, $S_{o,1}$ inside region 1 is calculated using Eq. (9). Condensate saturation in region 2, i.e., $S_{o,2}$ is calculated from CVD data, i.e., Eq. (11). The pressure P_1 can be calculated from Eq. (18) if the pore volume inside a given pressure contour is known. Mott (2003) defined a fractional pseudo pressure drawdown as:

$$\alpha = \frac{m(p) - m(p_w)}{m(p_R) - m(p_w)}$$
(20)

Tables of pore volume versus α inside a given pressure contour for different well types, geometry and reservoir geometry were set up. Using this table, the PV and ΔPV are calculated at any pressure that is used in Eq. (19).

Many combinations of the existing methods can be developed to obtain better results. Existing methods can be converted to iterative too. All other steps are the same as Fevang's Method. Xiao and Al-Muraikhi (2004) adopted Mott's method (Mott, 2003) with the modification of the material balance method to calculate the growth of the first region.

$$S_o = \frac{1}{\gamma}\left[1 - \frac{PV(P_1)}{PV_{tot}}\right]\int_0^t\left\{\left[\frac{1}{B_o(P_1)} - \frac{R_v(P_1)}{B_g(P_1)}\right]\right.$$
$$\left. \times \frac{\mu_g(P_1)B_g(P_1)}{K_{rg}}q_g^2\frac{\partial\alpha}{\partial(PV)}\frac{dR_v}{dP}\right\}dt$$
(21)

The gradient $\partial\alpha/\partial(PV)$ is calculated using Mott's (Mott, 2003) method. Therefore, pressure P_1 is obtained from Eqs. (9) and (21).

Gerami et al. (2010) introduced an iterative method coupled with general material balance calculation to avoid the necessity of production data in the original method of Fevang and Whitson (1996). For a given bottom hole pressure and time step, the average reservoir pressure and the pressure P_1 are guessed first. The gas and condensate flow rates are calculated independently. The flowing gas condensate ratio (R_v) is then determined by dividing the condensate flow rate by gas flow

rate. Pressure P_1 is obtained from PVT table using this flowing CGR to compare with the guessed value. If the error is in accepted range, average reservoir pressure is calculated from general material balance equation and compared to the guessed value. This iterative method is difficult to converge and very sensitive to PVT data.

Bonyadi et al. (2012) developed an iterative method that combined Mott's (Mott, 2003) and Xiao and Al-Muraikhi's methods (Xiao and Al-Muraikhi, 2004). The material balance used in all existing methods is only applicable to the depleted reservoir where average reservoir pressure is the characteristics feature.

A rate transient model considering a new linear flow is proposed to hydraulically fractured tight/shale systems with multiphase flow (of gas and condensate) and pressure-dependent rock/fluid properties with the combination of the dynamic drainage area (DDA), material balance, and decoupling of saturation and pressure (Qanbari and Clarkson, 2016) as shown in Eq. (22).

$$q_o = \frac{A_c\sqrt{k_i}}{57.16B_{oi}}\sqrt{\frac{\varphi_i c_{ti}}{\mu_{oi}t}}\left[m_o(\overline{p}_{inv}) - m_o(P_{wf})\right]$$
(22)

The pseudo-pressure in this study is defined in terms of dimensionless permeability, condensate viscosity, condensate formation volume factor as given in Eq. (23).

$$m_o(p) = \int_{p_o}^p\frac{\left(\frac{k}{k_i}\right)k_{ro}}{\left(\frac{\mu_o}{\mu_{oi}}\right)\left(\frac{B_o}{B_{oi}}\right)}dp$$
(23)

An iterative semi-analytical method (Behmanesh et al., 2017) for rate-transient analysis of gas condensate reservoirs coupled with the material balance is developed to calculate gas flow rate as shown in Eq. (24).

$$\frac{m(P_i) - m(P_{wf})}{q_g} = \frac{18.66}{kh}\ln\left(\frac{r_e}{r_{wa}} - \frac{3}{4}\right) + \frac{(1 - S_{wi})t_{ca}}{GB_{gi}\mu_{gi}c_{ti}}$$
(24)

Eq. (24) can also be utilized to estimate original gas in place. Two-phase material balance pseudotime is given by Eq. (25).

$$t_{ca} = \frac{\mu_{gi}c_{ti}}{q_g}\int_0^t\frac{q_g}{(\mu c_t)_{\text{two-phase}}}dt$$
(25)

These empirical methods are based on simplified reservoir model such as isothermal, homogeneous and isotropic reservoir with constant formation thickness or vertical fracture height with linear and boundary dominated flow. Therefore, it is not applicable for moving boundary flow with a long transient flow in most tight formations. One way to improve the model is to divide the reservoir into saturated and undersaturated segments (Velasco et al., 2016). In this semi-analytical model, the changes in the volume of these two segments were calculated using corresponding flow and phase properties coupled with the material balance method.

In most cases of empirical formulations, Darcy's law is assumed to be applicable and the impacts of capillary pressure,

gravity, high velocity of fluid, interfacial tensions, multi-physics transports are ignored. The existence of kerogen in shale plays a significant role in altering the PVT and flow properties (Pathak et al., 2015). Multi-physics models such as adsorption, the effect of confinement, and the presence of kerogen are also important for the modeling condensate flow in nanopores. There is considerable evidence that the known laws of adsorption, phase transitions, and flow are affected by nanometer-sized pores and the presence of kerogen. Therefore, the key challenge for future studies in developing an analytical or a semi-analytical model for condensate flow is to incorporate the multi-physics and geomechanics.

5. Summary

A vast amount of research efforts has been made for modeling gas-condensate flow. Understanding the thermodynamic and depletion natures are the key factors in developing a rigorous model. The division of pseudo pressure depending on the fluid phase is the key step in calculating the flow rate. It is advantageous to determine the modified black oil properties of gas-condensate fluid for model development. The calculations are very sensitive to PVT data. A detailed discussion of the model of gas-condensate flow is represented here including all the depletion states inside the reservoir.

The efficient model can replace the reservoir simulation for a rapid production forecast. Quick sensitivity study of parameters like matrix permeability, relative permeability, flowing bottom hole pressure, initial pressure, fluid properties can be conducted using this model. Methods can be developed using a combination of transient and pseudo-steady state conditions. This method is also useful for well inflow performance and material balance methods in unconventional reservoirs. This study provides a detailed discussion on PVT properties of gas-condensate, depletion mechanism in porous media, and analytical approaches in modeling flow in steady-state and pseudo steady-state conditions. The future research is to develop transient state flow models of gas-condensate in a tight formation such as shale with hydraulic fractures and horizontal well considering multiphysics and geomechanics.

Nomenclature

γ_g = Productivity index of gas, (RB/Day)(cp/psi)
$\Delta m(P)_g$ = Pseudopressure for gas, (SCF/RB)(psi/cp)
$\overline{p}_{inv}$ = Averagepressure in investigated volume, psi
μ = Viscosity, cp
μ_g = Gas viscosity, cp
μ_o = Oil or condensate viscosity, cp
μ_{oi} = Initial oil or condensate viscosity, cp
A_c = Total fracture area, ft^2
B = Formation volume factor, RB/SCF or RB/STB
B_{gd} = Dry gas formation volume factor, RB/SCF
B_o = Oil formation volume factor, RB/STB
B_{oi} = Initial oil formation volume factor, RB/STB
c_{ti} = Initial total compressibility, 1/psi
h = Formation thickness, ft
k = Absolute permeability, mD

k_i = Initial absolute permeability, mD
K_{rg} = Gas relative permeability, mD
K_{ro} = Oil relative permeability, mD
P = Pressure, psi
P_1 = Region 1 boundary pressure, psi
P_{dew} = Dew-point pressure, psi
P_e = Pressure at reservoir's outer boundary, psi
P_{eef} = Effective reservoir pressure, psi
P_i = Initial reservoir pressure, psi
P_R = Average reservoir pressure, psi
P_{wf} = Flowing bottom hole pressure, psi
q_g = Gas rate at well, SCF/day
q_{gw} = Gas flow rate at wellbore, SCF/day
q_o = Condensate rate at well, STB/day
$q_{o,max}$ = Maximum condensate rate, STB/day
R_p = Produced gas/condensate ratio, SCF/STB
R_s = Solution gas/condensate ratio, SCF/STB
R_{si} = Initial solution gas/condensate ratio, SCF/STB
R_v = Volatilized condensate/gas ratio, STB/MMSCF
R_{vf} = Flowing volatilized condensate/gas ratio, STB/MM-SCF
R_{vi} = Initial volatilized condensate/gas ratio, STB/MMSCF
S_o = Condensate saturation
$S_{o,1}$ = Condensate saturation in region 1
$S_{o,2}$ = Condensate saturation in region 2
S_{wc} = Irreducible water saturation
V_g = Gas volume in CVD and CCE tests, RB
V_L = Liquid volume in CVD and CCE tests, RB

Acknowledgement

Conflict of interest

The authors declare no competing interest.

References

Agarwal, R.G., Gardner, D.C., Kleinsteiber, S.W., et al. Analyzing well production data using combined type curve and decline curve analysis concepts. SPE Reservoir Eval. Eng. 1999, 2(5): 478-486.

Ahmed, T. Reservoir Engineering Handbook. Oxford, United Kingdom, Gulf Professional Publishing, 2010.

Amorim, T.C.A.D., Schiozer, D.J. Risk analysis speed-up with surrogate models. Paper SPE 153477 Presented at SPE Latin America and Caribbean Petroleum Engineering Conference, Mexico City, Mexico, 16-18 April, 2012.

Anifowose, F.A., Ewenla, A.O., Eludiora, S.I. Prediction of oil and gas reservoir properties using support vector ma-

chines. Paper IPTC-14514-MS Presented at International Petroleum Technology Conference, Bangkok, Thailand, 15-17 November, 2011.

Arps, J.J. Analysis of decline curves. Trans. AIME 1945, 160(1): 228-247.

Behmanesh, H., Hamdi, H., Clarkson, C.R. Production data analysis of gas condensate reservoirs using two-phase viscosity and two-phase compressibility. J. Nat. Gas Sci. Eng. 2017, 47: 47-58.

Bonyadi, M., Rahimpour, M.R., Esmaeilzadeh, F. A new fast technique for calculation of gas condensate well productivity by using pseudopressure method. J. Nat. Gas Sci. Eng. 2012, 4: 35-43.

Carreras, P.E., Turner, S.E., Wilkinson, G.T. Tahiti: Development strategy assessment using design of experiments and response surface methods. Paper SPE 100656 Presented at SPE Western Regional/AAPG Pacific Section/GSA Cordilleran Section Joint Meeting, Anchorage, Alaska, USA, 8-10 May, 2006.

Chen, Z., Huan, G., Wang, H. Computer simulation of compositional flow using unstructured control volume finite element methods. Computing 2006, 78: 31-53.

Clark, A.J., Lake, L.W., Patzek, T.W. Production forecasting with logistic growth models. Paper SPE 144790 Presented at SPE Annual Technical Conference and Exhibition, Denver, Colorado, USA, 30 October-2 November, 2011.

Clarkson, C.R., Qanbari, F., Nobakht, M., et al. Incorporating geomechanical and dynamic hydraulic-fracture-property changes into rate-transient analysis: Example from the haynesville shale. SPE Reservoir Eval. Eng. 2013, 16(3): 303-316.

Coleman, S., Wilde Jr., H.D., Moore, T.W. Quantitative effect of gas-oil ratios on decline of average rock pressure. Trans. AIME 1930, 86(1): 174-184.

Cook, R.E., Jacoby, R.H., Ramesh, A.B. A beta-type reservoir simulator for approximating compositional effects during gas injection. Soc. Pet. Eng. J. 1974, 14(5): 471-481.

Dahaghi, A.K., Esmaili, S., Mohaghegh, S.D. Fast track analysis of shale numerical models. Paper SPE 162699 Presented at SPE Canadian Unconventional Resources Conference, Calgary, Alberta, Canada, 30 October-1 November, 2012.

Dong, J.J., Hsu, J.Y., Wu, W.J., et al. Stress-dependence of the permeability and porosity of sandstone and shale from TCDP Hole-A. Int. J. Rock Mech. Min. Sci. 2010, 47(7): 1141-1157.

Dong, X., Liu, H., Hou, J., et al. Phase behavior of hydrocarbon mixtures in the organic nanopores of unconventional gas condensate reservoirs. Paper URTEC-2460485-MS Presented at SPE/AAPG/SEG Unconventional Resources Technology Conference, San Antonio, Texas, USA, 1-3 August, 2016.

Duong, A.N. An unconventional rate decline approach for tight and fracture-dominated gas wells. Paper SPE 137748 Presented at Canadian Unconventional Resources and International Petroleum Conference, Calgary, Alberta, Canada, 19-21 October, 2010.

Eilerts, C.K., Sumner, E.F., Potts, N.L. Integration of partial differential equation for transient radial flow of gas-condensate fluids in porous structures. Soc. Pet. Eng. J. 1965, 5(2): 141-152.

El-Sebakhy, E.M., Sheltami, T., Al-Bokhitan, S.Y. et al. Support vector machines framework for predicting the PVT properties of crude-oil systems. Paper SPE 105698 Presented at SPE Middle East Oil and Gas Show and Conference, Manama, Bahrain, 11-14 March, 2007.

Evinger, H.H., Muskat, M. Calculation of theoretical productivity factor. Trans. AIME 1942, 146(1): 126-139.

Fatt, I. The effect of overburden pressure on relative permeability. J. Pet. Technol. 1953, 5(10): 15-16.

Fatt, I., Davis, D.H. Reduction in permeability with overburden pressure. J. Pet. Technol. 1952, 4(12): 16.

Fetkovich, M.D., Guerrero, E.T., Fetkovich, M.J., et al. Oil and gas relative permeabilities determined from rate-time performance data. Paper SPE 15431 Presented at SPE Annual Technical Conference and Exhibition, New Orleans, Louisiana, 5-8 October, 1986.

Fetkovich, M.J. Decline curve analysis using type curves. J. Pet. Technol. 1980, 32(6): 1065-1077.

Fevang, Ø., Whitson, C.H. Modeling gas-condensate well deliverability. SPE Reservoir Eng. 1996, 11(4): 221-230.

Fussell, D.D. Single-well performance predictions for gas condensate reservoirs. J. Pet. Technol. 1973, 25(7): 860-870.

Gerami, S., Sadeghi, A., Masihi, M. New technique for calculation of gas condensate well deliverability. Paper SPE 130139 Presented at SPE Deep Gas Conference and Exhibition, Manama, Bahrain, 24-26 January, 2010.

Gondouin, M., Iffly, R., Husson, J. An attempt to predict the time dependence of well deliverability in gas condensate fields. Soc. Pet. Eng. J. 1967, 7(2): 113-124.

Guehria, F.M. Inflow performance relationships for gas condensates. Paper SPE 63158 Presented at SPE Annual Technical Conference and Exhibition, Dallas, Texas, 1-4 October, 2000.

Havlena, D., Odeh, A.S. The material balance as an equation of a straight line. J. Pet. Technol. 1963, 15(8): 895-900.

Ilk, D., Rushing, J.A., Perego, A.D., et al. Exponential vs. Hyperbolic decline in tight gas sands: Understanding the origin and implications for reserve estimates using Arps' decline curves. Paper SPE 116731 Presented at SPE Annual Technical Conference and Exhibition, Denver, Colorado, USA, 21-24 September, 2008.

Johnson, C., Jamiolahmady, M. Production data analysis using type curves in tight gas condensate reservoirs-impact of pressure-dependent permeability. Paper SPE 190832 Presented at SPE Europec featured at 80th EAGE Conference and Exhibition, Copenhagen, Denmark, 11-14 June, 2018.

Jones, J.R., Raghavan, R. Interpretation of flowing well response in gas-condensate wells (includes associated papers 19014 and 19216). SPE Form. Eval. 1988, 3(3): 578-594.

Kikani, J., Pedrosa Jr., O.A. Perturbation analysis of stress-sensitive reservoirs (includes associated papers 25281

and 25292). SPE Form. Eval. 1991, 6(3): 379-386.

Kniazeff, V.J., Nvaille, S.A. Two-phase flow of volatile hydrocarbons. Soc. Pet. Eng. J. 1965, 5(1): 37-44.

Labed, I., Oyeneyin, B., Oluyemi, G. Gas-condensate flow modelling for shale reservoirs. J. Nat. Gas Sci. Eng. 2018, 59: 156-167.

Li, B., Friedmann, F. Novel multiple resolutions design of experiment/response surface methodology for uncertainty analysis of reservoir simulation forecasts. Paper SPE 92853 Presented at SPE Reservoir Simulation Symposium, The Woodlands, Texas, 31 January-2 February, 2005.

Liu, L., Yao, J., Sun, H., et al. Compositional modeling of shale condensate gas flow with multiple transport mechanisms. J. Pet. Sci. Eng. 2019, 172: 1186-1201.

Mannon, R.W. Oil production forecasting by decline curve analysis. Paper SPE 1254 Presented at Fall Meeting of the Society of Petroleum Engineers of AIME, Denver, Colorado, 3-6 October, 1965.

McCain, W.D. The Properties of Petroleum Fluids. Tulsa, USA, PennWell Books, 2017.

McKee, C.R., Bumb, A.C., Koenig, R.A. Stress-dependent permeability and porosity of coal and other geologic formations. SPE Form. Eval. 1988, 3(1): 81-91.

Mead, H.N. Modifications to decline curve analysis. Trans. AIME 1956, 207(1): 11-16.

Millikan, C.V. Gas-oil ratio as related to the decline of oil production, with notes on the effect of controlled pressure. Trans. AIME 1926, G-26(1): 147-157.

Momeni, A., Dadvar, M., Hekmatzadeh, M., et al. 3D pore network modeling and simulation for dynamic displacement of gas and condensate in wellbore region. Int. J. Multiphase Flow 2017, 97: 147-156.

Mott, R. Engineering calculations of gas condensate well productivity. SPE Reservoir Eval. Eng. 2003, 6(5): 298-306.

Muskat, M. The production histories of oil producing gas-drive reservoirs. J. Appl. Phys. 1945, 16(3): 147-159.

O'Dell, H.G. Successfully cycling a low-permeability, high-yield gas condensate reservoir. J. Pet. Technol. 1967, 19(1): 41-47.

Okouma Mangha, V., Guillot, F., Sarfare, M., et al. Estimated ultimate recovery (EUR) as a function of production practices in the Haynesville shale. Paper SPE 147623 Presented at SPE Annual Technical Conference and Exhibition, Denver, Colorado, USA, 30 October-2 November, 2011.

Orangi, A., Nagarajan, N.R., Honarpour, M.M., et al. Unconventional shale oil and gas-condensate reservoir production, impact of rock, fluid, and hydraulic fractures. Paper SPE 140536 Presented at SPE Hydraulic Fracturing Technology Conference, The Woodlands, Texas, USA, 24-26 January, 2011.

Ostensen, R.W. The effect of stress-dependent permeability on gas production and well testing. SPE Form. Eval. 1986, 1(3): 227-235.

Palacio, J.C., Blasingame, T.A. Decline-curve analysis with type curves-Analysis of gas well production data.

Paper SPE 28688 Presented at International Petroleum Conference and Exhibition of Mexico, Veracruz, Mexico, 10-13 October, 1994.

Panja, P., Conner, T., Deo, M. Factors controlling production in hydraulically fractured low permeability oil reservoirs. Int. J. Oil, Gas Coal Technol. 2016, 13(1): 1-18.

Panja, P., Deo, M. Factors that control condensate production from shales: Surrogate reservoir models and uncertainty analysis. SPE Reservoir Eval. Eng. 2016, 19(1): 130-141.

Panja, P., Deo, M. Unusual behavior of produced gas oil ratio in low permeability fractured reservoirs. J. Pet. Sci. Eng. 2016, 144: 76-83.

Panja, P., Pathak, M., Deo, M. Productions of volatile oil and gas-condensate from liquid rich shales. Adv. Geo-Energy Res. 2019, 3(1): 29-42.

Panja, P., Pathak, M., Velasco, R., et al. Least square support vector machine: An emerging tool for data analysis. Paper SPE 180202 Presented at SPE Low Perm Symposium, Denver, Colorado, 5-6 May, 2016.

Pan, S., Ma, J., Zuo, J.Y., et al. A pore-scale mechanistic investigation of shale gas condensate at near saturation pressure on fluid flow in shale. Paper URTEC-2019-248-MS Presented at SPE/AAPG/SEG Unconventional Resources Technology Conference, Denver, Colorado, USA, 22-24 July, 2019.

Parikh, H. Reservoir characterization using experimental design and response surface methodology. USA, Texas A&M University, 2003.

Pathak, M., Deo, M., Panja, P., et al. The effect of kerogen-hydrocarbons interaction on the PVT properties in liquid rich shale plays. Paper SPE 175905 Presented at SPE/CSUR Unconventional Resources Conference, Calgary, Alberta, Canada, 20-22 October, 2015.

Pratikno, H., Rushing, J.A., Blasingame, T.A. Decline curve analysis using type curves-Fractured wells. Paper SPE 84287 Presented at SPE Annual Technical Conference and Exhibition, Denver, Colorado, 5-8 October, 2003.

Qanbari, F., Clarkson, C.R. Rate-transient analysis of liquid-rich tight/shale reservoirs using the dynamic drainage area concept: Examples from north american reservoirs. J. Nat. Gas Sci. Eng. 2016, 35: 224-236.

Raghavan, R., Scorer, J.D.T., Miller, F.G. An investigation by numerical methods of the effect of pressure-dependent rock and fluid properties on well flow tests. Soc. Pet. Eng. J. 1972, 12(3): 267-275.

Rushing, J.A., Perego, A.D., Sullivan, R., et al. Estimating reserves in tight gas sands at hp/ht reservoir conditions: Use and misuse of an arps decline curve methodology. Paper SPE 109625 Presented at SPE Annual Technical Conference and Exhibition, Anaheim, California, 11-14 November, 2007.

Santos, M.P.P.C., Carvalho, M.S. Pore network model for retrograde gas flow in porous media. J. Pet. Sci. Eng. 2020, 185: 106635.

Schilthuis, R.J. Active oil and reservoir energy. Trans. AIME 1936, 118(1): 33-52.

Tarner, J. How different size gas caps and pressure maintenance programs affect amount of recoverable oil. Oil

Wkly. 1944, 144(2): 32-44.

Thomas, R.D., Ward, D.C. Effect of overburden pressure and water saturation on gas permeability of tight sandstone cores. J. Pet. Technol. 1972, 24(2): 120-124.

Thompson, J.M., Nobakht, M., Anderson, D.M. Modeling well performance data from overpressured shale gas reservoirs. Paper SPE 137755 Presented at Canadian Unconventional Resources and International Petroleum Conference, Calgary, Alberta, Canada, 19-21 October, 2010.

Thornton, O.F. Gas-condensate reservoirs-a review. Paper API-46-150 Presented at Drilling and Production Practice, New York, 1 January, 1946.

Tracy, G.W. Simplified form of the material balance equation. Trans. AIME 1955, 204(1): 243-246.

Vairogs, J., Hearn, C.L., Dareing, D.W., et al. Effect of rock stress on gas production from low-permeability reservoirs. J. Pet. Technol. 1971, 23(9): 1161-1167.

Valko, P.P. Assigning value to stimulation in the Barnett Shale: A simultaneous analysis of 7000 plus production hystories and well completion records. Paper SPE 119369 Presented at SPE Hydraulic Fracturing Technology Conference, The Woodlands, Texas, 19-21 January, 2009.

Velasco, R., Panja, P., Deo, M. New production performance and prediction tool for unconventional reservoirs. Paper URTEC-2461718-MS Presented at SPE/AAPG/SEG Unconventional Resources Technology Conference, San Antonio, Texas, USA, 1-3 August, 2016.

Whitson, C.H., Sunjerga, S. PVT in liquid-rich shale reservoirs. Paper SPE 155499 Presented at SPE Annual Technical Conference and Exhibition, San Antonio, Texas, USA, 8-10 October, 2012.

Xiao, J.J., Al-Muraikhi, A.J. A new method for the determination of gas condensate well production performance. Paper SPE 90290 Presented at SPE Annual Technical Conference and Exhibition, Houston, Texas, 26-29 September, 2004.

Xiong, Q., Baychev, T.G., Jivkov, A.P. Review of pore network modelling of porous media: Experimental characterisations, network constructions and applications to reactive transport. J. Contam. Hydrol. 2016, 192: 101-117.

Yang, S., Wu, K., Xu, J., et al. Roles of multicomponent adsorption and geomechanics in the development of an eagle ford shale condensate reservoir. Fuel 2019, 242: 710-718.